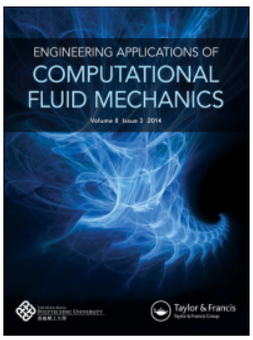

Taylor & Francis
Taylor & Francis Group

Engineering Applications of Computational Fluid Mechanics

ISSN: (Print) (Online) Journal homepage: https://www.tandfonline.com/loi/tcfm20

Research on the hull form optimization using the surrogate models

Shenglong Zhang, Tahsin Tezdogan, Baoji Zhang & Ling Lin

To cite this article: Shenglong Zhang, Tahsin Tezdogan, Baoji Zhang & Ling Lin (2021) Research on the hull form optimization using the surrogate models, Engineering Applications of Computational Fluid Mechanics, 15:1, 747-761, DOI: 10.1080/19942060.2021.1915875

To link to this article: https://doi.org/10.1080/19942060.2021.1915875

Published online: 03 May 2021.

ENGINEERING APPLICATIONS OF COMPUTATIONAL FLUID MECHANICS
2021, VOL. 15, NO. 1, 747–761
https://doi.org/10.1080/19942060.2021.1915875

Taylor & Francis
Taylor & Francis Group

Research on the hull form optimization using the surrogate models

Shenglong Zhang [a], Tahsin Tezdogan [b], Baoji Zhang[c] and Ling Lin[a]

[a]Department of Automotive Engineering, Changshu Institute of Technology, Changshu, People's Republic of China; [b]Department of Naval Architecture, Ocean and Marine Engineering, University of Strathclyde, Glasgow, UK; [c]Department of Ocean Environment and Engineering, College of Ocean Environment and Engineering, Shanghai Maritime University, Shanghai, People's Republic of China

ABSTRACT

The ship hull form optimization using the Computational Fluid Dynamics (CFD) method is increasingly employed in the early design of a ship, as an optimal ship hull form can obtain good hydrodynamics. However, it is time-consuming due to its many CFD simulations for the optimization. This paper presents a ship hull form optimization loop using the surrogate model, deep belief network (DBN), to reduce the wave-making resistance of the Wigley ship. The prediction performance of the wave-making resistance of the Wigley ship using the DBN method is discussed and compared with the traditional surrogate models found in this study. The results show that the resistance obtained using the deep belief network algorithm is superior to that obtained using the typical surrogate models. Then, a ship hull form optimization framework is built by integrating the Free From Deformation, non-linear programming by quadratic Lagrangian and deep belief network algorithms. The optimization results show that the deep belief network-based ship hull form optimization loop can be used to optimize the Wigley ship. The study presented in this paper could provide a deep learning algorithm for the ship design optimization.

ARTICLE HISTORY
Received 12 August 2020
Accepted 7 April 2021

KEYWORDS
Ship hull form optimization; surrogate model; wave-making resistance; deep belief network

1. Introduction

Wave-making resistance is one of the most important factors to be considered when a ship is in the early hull form design stage. This is because an optimal hull form has low wave-making resistance, which in turn decreases fuel consumption. With the development of computer techniques and mathematical algorithms, the Computational Fluid Dynamics (CFD) method has been extensively adopted to evaluate ship hydrodynamics in seas. However, this method is very time-consuming owing to its slow convergence rate. This problem inevitably complicates ship hull form optimization by the CFD method. Therefore, it is necessary for designers to explore a more efficient surrogate model for ship hull form optimization. The most common surrogate models include kriging models, Radial Basis Function (RBF) and neural networks. To find the mechanics between the ship performance indicators and the thickness of ship components, Deng (2014) employed the Back Propagation (BP) neural network to approximate the von-mises stress and max-shear stress for a ship powerboat. Lin et al. (2018) used the kriging model to optimize the twin-skeg ship and obtain the optimal hull form with the lowest total resistance. To reduce the number of CFD-based simulations, Baar et al. (2015) developed a new multi-fidelity Kriging surrogate model to carry out the uncertainty quantification analysis for a sailing yacht hull. Zhang, Zhang, Tezdogan, et al. (2018) employed the Elman method to approximate the total resistance of a DTMB 5512 ship. Ozcanan and Atahan (2019) used an RBF surrogate model to optimize guardrails, which provided an economic advantage of 23% compared to the original model. To solve the auto-berthing control problem, Zhang, Zhu, et al. (2019) developed a new auto-berthing control law integrating the adaptive neural network, and then a Cybership 2 ship was selected to discuss the feasibility of the control scheme in their study. Miao and Wan (2019) also used the kriging model to predict the total resistance of S60 ship. Bakhtiari and Ghassemi (2020) used the feedforward neural networks to calculate the hydrodynamic coefficients of thrust and torque of the marine cycloidal propeller. Kim et al. (2020) selected the artificial neural network to predict the ice resistance of the ship using different variables. Ye et al. (2020) used the BP neural network to approximate the total resistance of a 46,000t oil tanker, and then developed a ship design optimization method to optimize the bow and stern of the oil tanker, integrating the RBF interpolation surface modification method and particle swarm optimization algorithm. These popular methods are suitable for the

CONTACT Ling Lin linlingnl@163.com

data forecast and are expected to improve the optimization efficiency. However, with the development of the surrogate model, deep learning methods have gained much attention in recent years. The DBN method is a novel method that has been extensively applied for the prediction of different data. Yang and Zhong (2016) used the Deep Belief Network (DBN) method to forecast hospital outpatients and achieved 96% success. Li et al. (2019) used the DBN method to predict short-term traffic flow using supervised learning techniques. Bu et al. (2017) employed the DBN method for enhancer prediction and it was found to be effective in increasing the accuracy of enhancer prediction. Dong et al. (2020) developed a new forecasting model for the vibration performance of rolling mills using the DBN algorithm. In their studies, the DBN algorithm was used to predict the vibration intensity of the rolling mills according to the rolling parameters. The results shown that the error between the DBN method and the experimental data was only 3.94%. Jia et al. (2020) used the DBN algorithm to predict the bounced landing of the aircraft. Considering the influence of the airport environment, the prediction accuracy using the DBN method was up to 94.78%. Li, Zhao, et al. (2020) employed an improved DBN algorithm to predict the oxygen consumption. Six parameters were set as the input data, the oxygen consumption was selected as the output data. Finally, the average percentage error between the original data and prediction data using the improved DBN method was only 1.92%. Li, Liang, et al. (2020) developed a prediction method for the performance of the short-term power generation using the DBN-based PSO method. The grey correlation degree method was employed to design the sample data firstly. Then the revised sample data was used to establish the DBN-based PSO model. After the completion of the prediction, the results showed that the mean absolute percentage error between the DBN-based PSO model and sample data was only 3.45%. As can be seen from the above literature, the prediction accuracy using the DBN algorithm is relatively high for different optimization fields. It can be deduced that the DBN algorithm is a good method to predict different kinds of sample data. However, there have not been any specific ship resistance prediction and optimization studies that employ a DBN-based surrogate model. Therefore, a comparative analysis of BP, Elman, RBF and DBN methods is performed to evaluate their wave-making resistance prediction performance. Then, the optimal surrogate model is employed to optimize the Wigley ship in terms of resistance reduction, thereby improving its overall efficiency.

Surface modification is a key part of the shape optimization and design problem. The Free Form Deformation (FFD) method is a good geometry reconstruction method for deforming the 3D geometry model. It has been widely used in the different optimization fields (Guo et al., 2020; Xu et al., 2019; Yu et al., 2016; Zhang, Zhang, Yang, et al., 2018). Garg et al. (2017) used the FFD method to change the hydrofoil surface with 200 control points. Wang et al. (2018) employed the FFD method to deform the hydrofoil using several control points moved along the y-direction. Meng et al. (2019) selected 10 points to change the geometry of an airfoil aerodynamic. Li, Wang, et al. (2020) used three design variables to deform the shape of a blendedwing-body (BWB) underwater glider using the FFD method. Song et al. (2020) selected the FFD method to change the airfoil torsion angle and chord length of a propeller, and the RBF method to regenerate meshes of the original propeller. For the ship hull form optimization, Cheng et al. (2018) and Wei et al. (2019) applied RBF interpolation to alter the Series 60 ship and KRISO Container Ship (KCS) ship. The B-spline function method was selected by Zhang and Zhang (2015) to deform the hull lines of a Series 60 ship. Zhang, Chen, et al. (2019) used the full parametric method, implemented on CAESES, to modify a drilling ship. Miao and Wan (2019) employed an FFD technique to deform the bulbous bow and the stern of an S60 ship. As the good performance of the FFD method in the ship hull form deformation, this study employed the FFD method to alter the ship hull geometry with two design variables.

Firstly, the BP, Elman, RBF and DBN algorithms were employed in this paper to predict the wave-making resistance. Then, the prediction accuracy for different surrogate models was compared and discussed. Following this, the ship optimization platform for the Wigley ship was built, integrating the FFD and DBN and CFD methods. In the optimization, many uncertainty factors can lead to significant differences in the optimization results (Hou et al., 2016). Therefore, the interval number method, as proposed by Hou et al. (2016), was used in this study to discuss the uncertainty optimization problem considering the influence of the ship speeds. In this paper, Section 2 shows the ship geometry of the Wigley ship used in this study. Section 3 shows the ship hull form optimization problem, including the objective function and design variables, constraints and optimization flowchart. In Section 4, the optimization methods, including the geometry reconstruction, optimizer and resistance evaluation method are shown. At the same time, the verification of the XPAN model method is carried out to predict the wave-making resistance of the Wigley ship. Section 5 describes the construction of the surrogate models and the accuracy assessment that is performed to verify the reliability of the DBN-based resistance prediction model. Then, Section 6 presents the example of the ship hull

Table 1. Wigley main properties.

Dimensions	Value (m)
L_{pp}	2.00
Breadth	0.20
Draft	0.125

form optimization using the Wigley ship. The optimization results for certainty and uncertainty methods are also compared and discussed in this section. Finally, the results of this study and suggestions for future work are shown in Section 7.

2. Ship geometry

A Wigley ship is used as the research objective in this study. The ship hull form formula can be written as:

$$y = \frac{B}{2}\left[1 - \left(\frac{2x}{L}\right)^2\right]\left[1 - \left(\frac{z}{d}\right)^2\right] \tag{1}$$

Table 1 shows the main properties of the Wigley ship. Lan (2012) pointed out that the Wigley ship is always optimized to reduce the wave-making resistance as wave contours on the free surface are very small. Therefore, the wave-making resistance of the Wigley ship is set as optimization objective parameter in this study.

3. Optimization problem

3.1. Objective function

As shown in Section 2, the wave-making resistance R_W is set as the objective function at design speed $Fr = 0.35$. The wave-making resistance coefficient C_W is used to express the calculation results of the R_W in the following sections.

3.2. Design variables and constraints

Only the port side of the Wigley ship is used for the numerical calculation in order to improve the CFD computing efficiency. First of all, a control volume is established around the original Wigley ship hull with some points and connections, as shown in Figure 1. The first half of the hull is fixed, while the second half of the hull is set as the optimization region. For the ship hull form optimization, two design variables are used to change the second half of the hull geometry. Table 2 shows the design variables used in this study. Four points can be moved along the y-axis to deform the ship surface, and two design variables (a and b) are selected to show the moved distance for these four points. Considering the size of the Wigley ship, the movement scope of a and b ranges from −0.35 to 0.35. The displacement is fixed by changing the draft of the deformed ship.

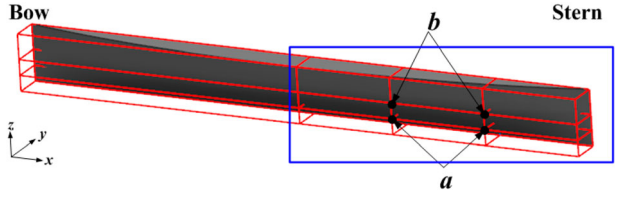

Figure 1. The optimization position for the Wigley ship.

Table 2. The design variables and its movement scope.

Design variables	a	b
Constraints	$-0.035 \leq a \leq 0.035$	$-0.035 \leq b \leq 0.035$

3.3. Optimization flowchart

The NLPQL method is selected as the optimization algorithm to optimize the second half of the Wigley ship geometry with two design variables. The surrogate model is employed to approximate the wave-making resistance for different deformed ship hulls. Figure 2 shows the ship hull form optimization flowchart, the optimization steps can be summarized as:

(1) Deform the ship hull geometry using the FFD method by using two design variables.

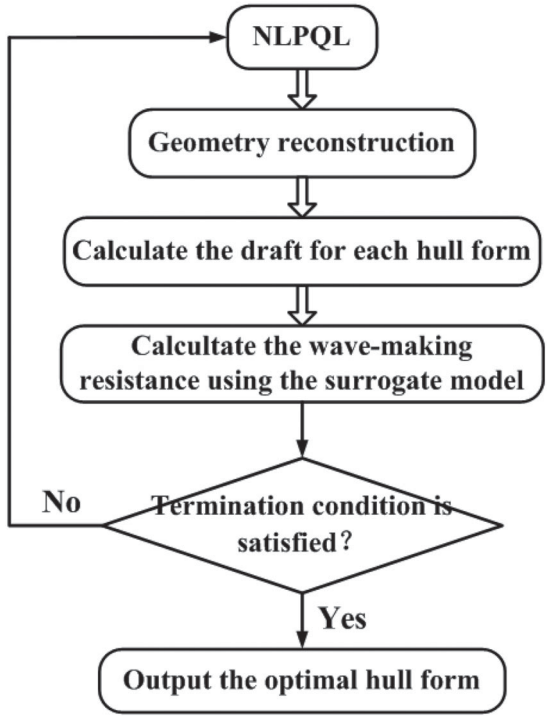

Figure 2. A ship hull form optimization flowchart.

(2) Calculate the draft for each new ship hull.
(3) Calculate the C_W by using a different surrogate model.
(4) Change the two design variables using the NLPQL method, and repeat Steps (1)–(4) until the termination condition is met.

4. Optimization methods

In the construction of a ship optimization method, three main structures are essential: the optimization method, the geometry reconstruction and the calculation method for the ship's resistance, as shown in Figure 3. Therefore, the following sections respectively show the geometry reconstruction method, optimizer and resistance evaluation method.

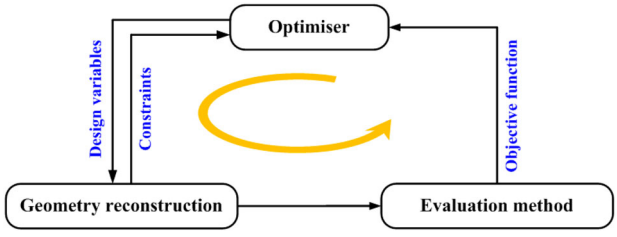

Figure 3. A ship hull form optimization platform.

4.1. Geometry reconstruction

The geometry reconstruction is the central section to obtain suitable deformed ship hulls. In this study, the FFD method is used to deform the geometry of the Wigley ship, as it has been extensively used in different fields (Chen et al., 2019; Li et al., 2016; Liu, 2019; Miao et al., 2020; Shen et al., 2020; Yang, 2020), obtaining good results. This method can deform the ship geometry easily. In order to show the deformation effect for the original Wigley ship, two examples of the ship hull form deformation have been made using the maximum ($a = -0.035, b = -0.035$) and minimum ($a = 0.035,\ b = 0.035$) boundaries. Figure 4 shows a comparison of the cross-section and longitudinal section for original and deformed hulls. According to the figure, the deformed ship surface is outward expansion for the design variables: $a = -0.035,\ b = -0.035$ in the Figure 4(a) and inward shrinkage for the design variables: $a = 0.035,\ b = 0.035$ in Figure 4(b). Therefore, this method is used to change the Wigley ship geometry in order to obtain the deformed ships for the hull form optimization in the following sections.

4.2. Optimizer

The NLPQL algorithm is selected as the optimization method to find the optimal ship which is similar to the original ship. It is an improved Sequential Quadratic

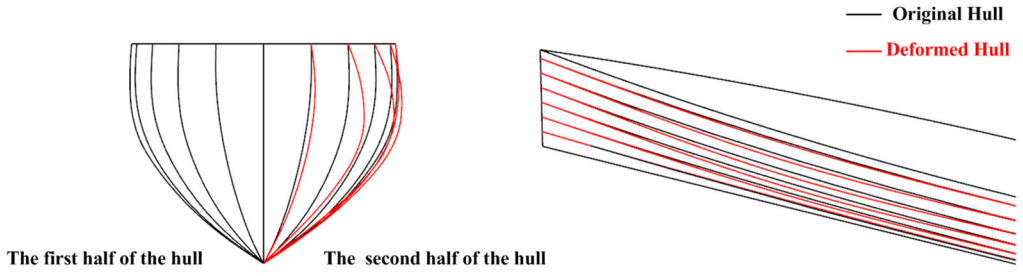

(a) The hull lines with the design variables: a=-0.035, b=-0.035 and original hull

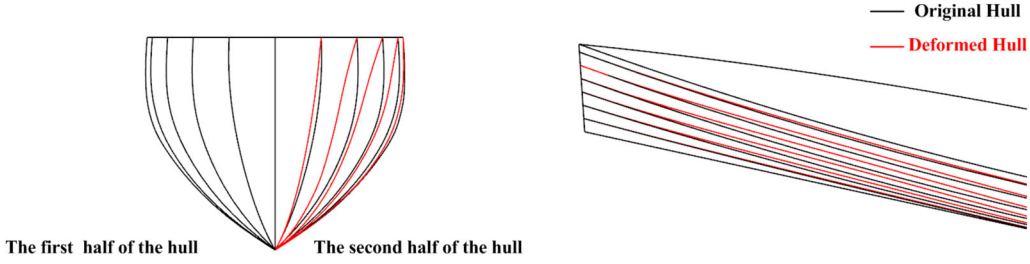

(b) The hull lines with the design variables: a=0.035, b=0.035 and original hull

Figure 4. The hull lines for different design variables for different hulls. (a) The hull lines with the design variables: $a = -0.035$, $b = -0.035$ and original hull and (b) the hull lines with the design variables: $a = 0.035$, $b = 0.035$ and original hull

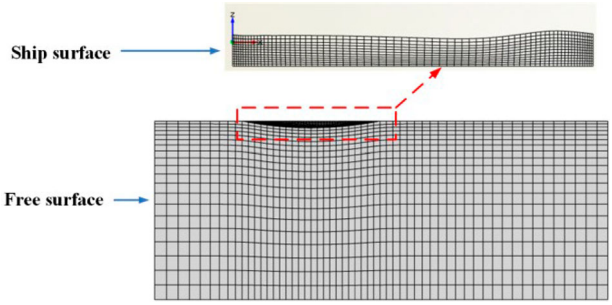

Figure 5. The mesh on the free surface and ship hull surface.

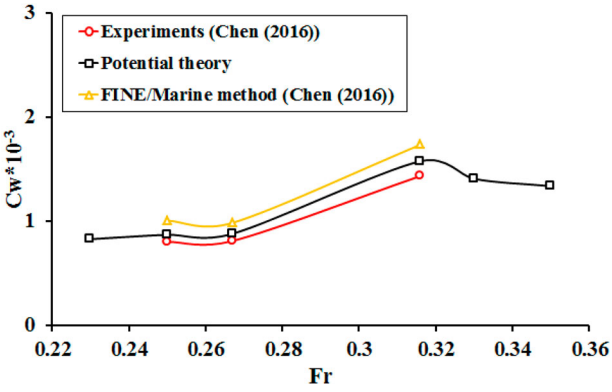

Figure 6. C_W changes with *Fr*.

Programming method, with an additional linear searching. In this algorithm, the Broyden-Fletcher-Goldfarb-Shanno (BFGS) method is employed to update the matrix.

4.3. Resistance evaluation method

4.3.1. CFD method

The potential theory, that is, the Rankine-source method is selected to calculate the C_W of the Wigley ship. All calculations are performed using the XPAN module on the SHIPFLOW software. Figure 5 shows the mesh on the free surface and on the ship hull surface. The total number of the panels is 1996, and the total number of the nodes is 2159 for the current computational model. Figure 6 shows a summary of the C_W that was obtained using XPAN module and FINE/Marine method (Chen, 2016) and the experimental data (Chen, 2016). According to the figure, the wave-making resistance coefficients obtained by the XPAN module and FINE/Marine method (Chen, 2016) are found to be inconsistent with the EFD value (Chen, 2016). While the average deviation of the wave-resistance is reduced by 13.65% using the XPAN module at $Fr = 0.25$, 0.267 and 0.316 compared to the results obtained by using the FINE/Marine model. It can be found that the C_W obtained using the

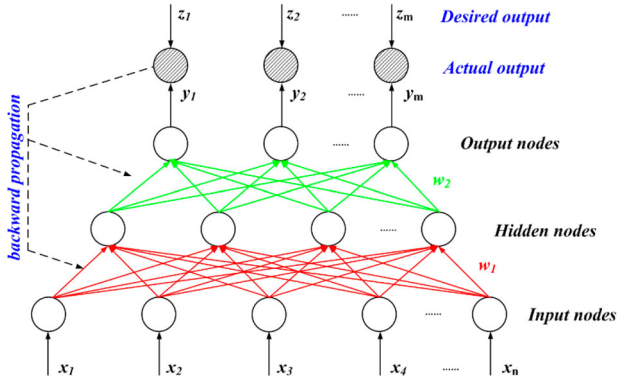

Figure 7. The BP neural network (Han, 2007).

XPAN module method is better than that obtained by the FINE/Marine method from Chen (2016). Therefore, the SHIPFLOW software is employed to calculate the C_W for different deformed ships at different speeds in this study.

4.3.2. Surrogate models

The surrogate model is a suitable method for improving the wave-making resistance prediction efficiency for a Wigley ship compared to the CFD method. In this study, four surrogate models are employed and discussed for the wave-making prediction. Therefore, the following section shows the four surrogate models used in this study.

4.3.2.1. BP method. The BP method is a typical feedforward network. Figure 7 shows an example of the three layers BP neural network (Han, 2007). The sigmoid function is set as the activation function in this algorithm. The optimal prediction data can be obtained by continuously adjusting the backward propagation errors between the actual output values y_m and desired output values z_m (Han, 2007).

4.3.2.2. Elman method. Different from the BP method, the Elman method includes four typical neural networks. Figure 8 presents the structure of the Elman method (Shi, 2006). The input layer is used to transmit the signal of the initial sample data x_n, and the output layer plays the role

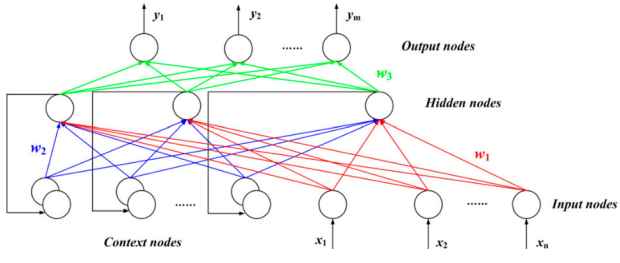

Figure 8. The Elman neural network (Shi, 2006).

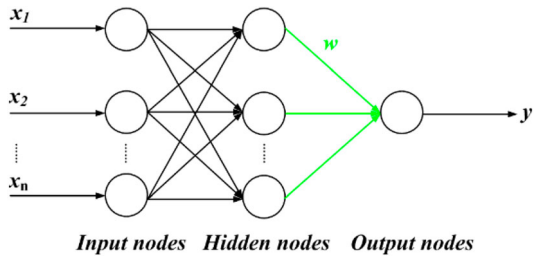

Figure 9. The RBF neural network (Feng & Lu, 2010).

of the linear weighting, which is the same as the BP neural network. The context layer, a special layer in the Elman algorithm, can memorize the first output data of the hidden layer and then return back to hidden layer in order to improve the performance of processing the dynamic information (He, 2016).

4.3.2.3. RBF method. The structure of the RBF method can be found in Figure 9 (Feng & Lu, 2010). The input layer also carries out the signal transmission for the original samples data x_n, like the input layer of the BP and Elman neural networks. The non-linear transformation is carried out firstly, then the linear transformation is conducted in this algorithm (He, 2016). Finally, the output layer is used to adjust the linear weights of the RBF method. For the hidden layer, the Gauss function is set as activation function.

4.3.2.4. DBN method. The DBN method is a multilayer probabilistic generative model developed by Hinton et al. (2006), which is constructed by a great number of Restricted Boltzmann Machines (RBM) models (Feng, 2015). The RBM model includes hidden and visible layers (as shown in Figure 10). The energy of joint configuration between the visible and hidden layers can be defined as (Shan, 2015):

$$E(v,h|\theta) = -\sum_{i=1}^{n}\sum_{j=1}^{m} v_i w_{ij} h_j - \sum_{i=1}^{n} c_i v_i - \sum_{j=1}^{m} d_j h_j \quad (2)$$

where v_i and h_j are binary states, w_{ij} are connection weights, c_i and d_j are biases.

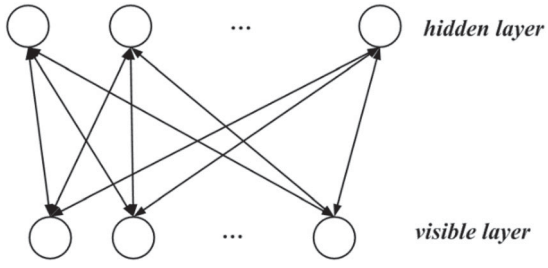

Figure 10. The RBM model (Bengio, 2009).

The joint distribution can be expressed as (Zhang, 2016):

$$P(v,h|\theta) = \frac{1}{Z(\theta)} e^{-E(v,h|\theta)} \quad (3)$$

$$Z(\theta) = \sum_{v}\sum_{h} e^{-E(v,h|\theta)} \quad (4)$$

where $Z(\theta)$ is the partition function.

According to Equations (2)–(4), the individual activation probability of h_j given visible layer, or v_i given hidden layer can be obtained by (Wang, 2015):

$$P(h_j = 1|v,\theta) = \sigma(d_j + \sum_{i=1}^{n} v_i w_{ij}) \quad (5)$$

$$P(v_i = 1|h,\theta) = \sigma(c_i + \sum_{j=1}^{m} h_j w_{ij}) \quad (6)$$

The DBN algorithm, a new unsupervised learning model, is different from the other three neural networks since it includes two training steps in order to obtain accurate prediction results. Many RBM models are included in the first training step. The first RBM model is trained using the Contrastive Divergence algorithm in order to obtain the hidden layer parameters (Li, 2014). Then, the second RBM model is trained using the hidden layer parameters of the first RBM model (Li, 2014). After pre-training all the RBM models using the Contrastive Divergence algorithm in the pre-training step, the BP neural network is used to adjust the parameters and improve the prediction accuracy of the DBN model in fine-tuning step (Li, 2014). After the completion of these two steps, the training process of the DBN method is completed.

5. The accuracy evaluation for surrogate models

5.1. Evaluation criteria

The RMSE and MAE and multiple correlation coefficient R-square (R^2) are used to verify the reliability of the approximate model. The formula can be written as:

$$\mathrm{RMSE} = \sqrt{\frac{1}{n}\sum_{i=1}^{n}(Sur_i - Pot_i)^2} \quad (7)$$

$$\mathrm{MAE} = \frac{1}{n}\sum_{i=1}^{n}|Sur_i - Pot_i| \quad (8)$$

$$R^2 = 1 - \frac{\sum_{i=1}^{n}(Pot_i - Sur_i)^2}{\sum_{i=1}^{n}(Pot_i - Ave)^2} \quad (9)$$

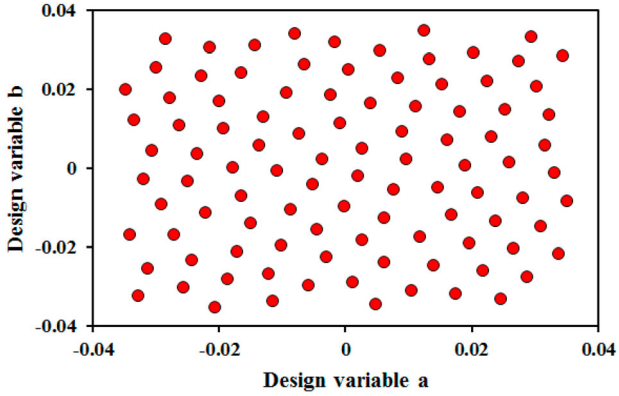

Figure 11. The two dimension spatial distribution for 100 sample ships.

where Pot_i is the i-th C_W obtained using potential theory (XPAN model), Ave is the average value of Pot_i, Sur_i is the i-th C_W obtained using the surrogate model. While the smaller the RMSE and MAE, the higher is the prediction accuracy. If the value of R^2 is closer to 1, the prediction accuracy of the surrogate model is higher.

5.2. Data preparing

In order to obtain suitable samples, the Opt LHD method is employed in this study to obtain the sample data in the ship hull form optimization space. Table 3 shows the 100 sample ships data, as well as the corresponding draft and the C_W. The C_W for the sample ships is calculated by using the potential theory in the Section 4.3.1. Figure 11 shows the sample ships distribution in the fix ship hull form optimization space. For obtaining the samples in the multi-dimensional fixed optimization space using the design of the experiment method, the noise data seems inevitable (Huang, 2018). In order to obtain suitable sample data, the median absolute deviation (MAD) method is employed in this paper to smooth the noisy sample data. Since the sample data for variable b is not changed, Figure 12 only shows the results of the revised data using the MAD method for the variable a and the objective function C_W. The red points in the figure are the original data obtained using the Opt LHD method that needs to be revised. The black lines show the revised sample data using the MAD method.

5.3. Establishment of the surrogate models

The parameters of the surrogate models have a great influence on the calculation results. For different surrogate models, the selection of parameters is very complicated. With the improvement of the mathematical theory, this problem can be solved using optimization

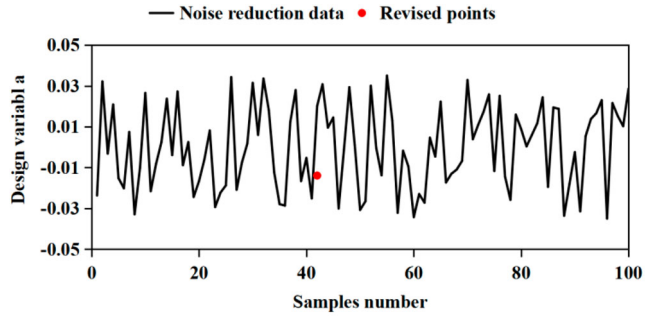

(a) The filter noise for the design variable a

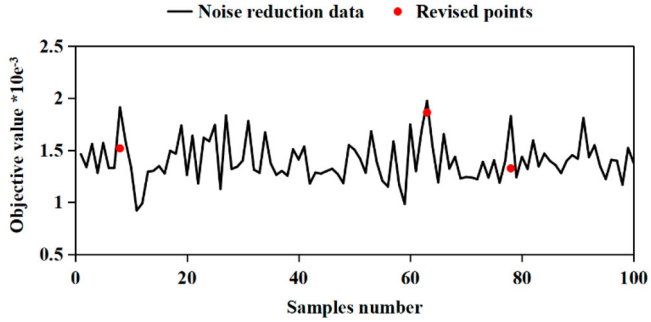

(b) The filter noise for the objective function C_W

Figure 12. The filter noise for the sample ships data using the MAD method. (a) The filter noise for the design variable a and (b) The filter noise for the objective function C_W.

Table 3. Sample ships obtained using Opt LHD method, including the corresponding draft and C_W.

No.	a	b	Draft	C_W calculated by potential theory
1	−0.02369	0.00389	0.12341	0.0014617
2	0.03217	0.01379	0.12874	0.0013377
3	−0.00318	−0.02227	0.12317	0.0015592
4	0.02086	−0.00601	0.12621	0.0012815
5	−0.0152	−0.01379	0.12284	0.0015683
…	…	…	…	…
96	−0.0046	−0.0152	0.1235	0.0015288
97	0.02227	0.02227	0.12863	0.0011911
98	−0.01732	−0.02086	0.12218	0.0016535
99	−0.01308	0.01308	0.12497	0.0013228
100	−0.01096	−0.00035	0.12411	0.0014359

technology. As the particle swarm optimization (PSO) algorithm is a good global optimization method using in the different optimization problems (Moradi et al., 2020; Song et al., 2021; Yadav & Anubhav, 2020; Zhang et al., 2021), a PSO algorithm is employed in this study to find the optimal parameters for different surrogate models with the k-fold cross-validation method (Zhou et al., 2017). The optimization step can be summarized as follows:

(1) Define the variables (parameters of the surrogate model) and the PSO parameters.
(2) Generate a set of variables randomly using the PSO algorithm.

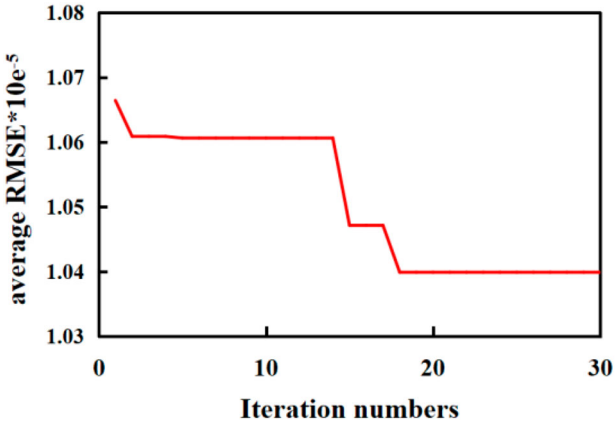

Figure 13. The parameters optimization for BP neural network.

(3) The samples data is divided into ten parts, one part is set as validation set sequentially, the other nine parts are set as the training set to train the surrogate model.
(4) Establish the surrogate model using the parameters obtained by Step (2) and then obtain the prediction values.
(5) Calculate the RMSE value 10 times using Equation (7). Then calculate the average RMSE value.
(6) Repeat Step (2) to Step (5) until the termination condition is satisfied.
(7) Output the optimal parameters for different surrogate models with the minimum average RMSE value.

As the number of neurons in the hidden layer and the learning rate is very important for the prediction results of the BP neural network, these two parameters are optimized. Figure 13 shows the optimization iterative process for the BP neural network parameters.

The number of the hidden layer are always determined using Equation (10) (Li et al., 2015). For the current Elman neural network, two variables (a and b) are selected as the input values, and one variable (wave-making resistance coefficient) is set as the output value. Therefore, the number of the hidden layer is from 3 to 12. Figure 14 shows the average RMSE value changes with the hidden layers. According to the figure, the average RMSE value increased firstly, then decreased. Finally, the average RMSE value was the lowest when the hidden layer was set as 12. Therefore, the hidden layer was selected as 12 to carry out the prediction of the wave-making resistance of the Wigley ship.

$$n_{\text{layers}} = \sqrt{n_{\text{input}} + n_{\text{output}}} + \eta \tag{10}$$

where n_{layers} represent the number of the hidden layer, n_{input} is the number of the input variables, n_{output} is the number of the output variables and η is the parameter from 1 to 10.

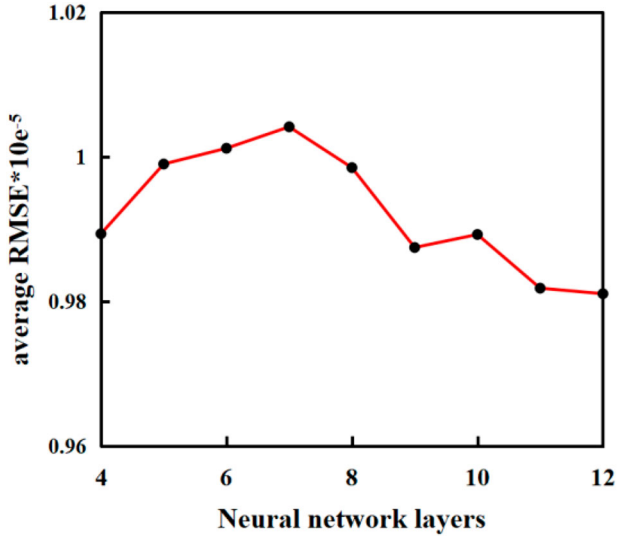

Figure 14. The average RMSE value changes with network layers for Elman neural network.

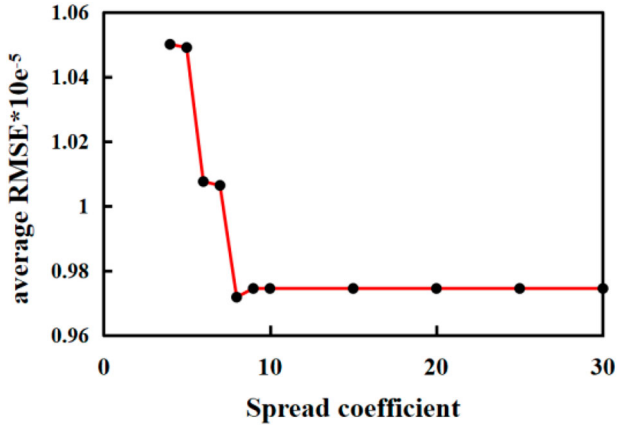

Figure 15. The average RMSE value changes with spread coefficient for RBF algorithm.

For the RBF neural network, the selection of the spread coefficient is very important for the calculation results. Figure 15 shows the average RMSE value changes with the spread coefficient. The average RMSE value is the lowest when the spread coefficient is bigger than 9. With the increase of the spread coefficient, the prediction accuracy is increased firstly. When the spread coefficient is upper to 9, the prediction accuracy tends to stabilize.

For the DBN algorithm, the learning rate and the momentum are set as the optimization variables. After the completion of the optimization, the minimum average RMSE has been obtained. Figure 16 shows the optimization iteration history for the learning rate and the momentum.

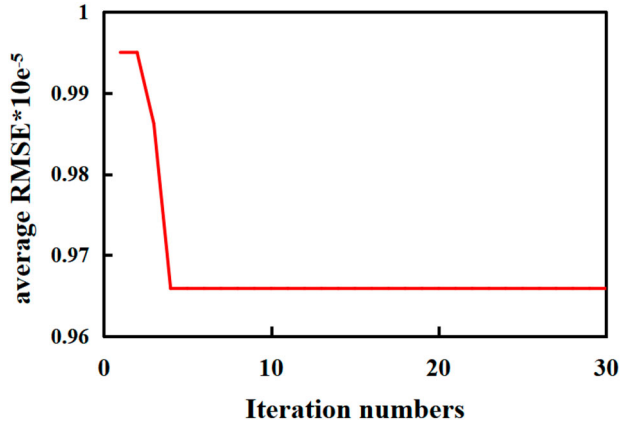

Figure 16. The parameters optimization for DBN algorithm.

Table 4. A comparison of average RMSE value for the surrogate model training.

Surrogate model	BP method	Elman method	RBF method	DBN method
Average RMSE	1.4 e^{-05}	0.981 e^{-05}	0.975 e^{-05}	0.966 e^{-05}

Table 4 summarizes the average RMSE value for the different surrogate model training. As can be seen from the table, the BP method has the largest average RMSE value, while the DBN method shows the lowest average RMSE value. It can be deduced that the DBN method has the best prediction accuracy, while the BP method shows the worst prediction accuracy for the wave-making resistance of the Wigley ship.

5.4. Accuracy verification for different surrogate models

To further verify the prediction accuracy for different neural networks, an Opt LHD algorithm is employed to design another 20 sample ships, as shown in Figure 17. Table 5 shows the test samples, as well as the corresponding draft and wave-making resistance coefficient C_W. The

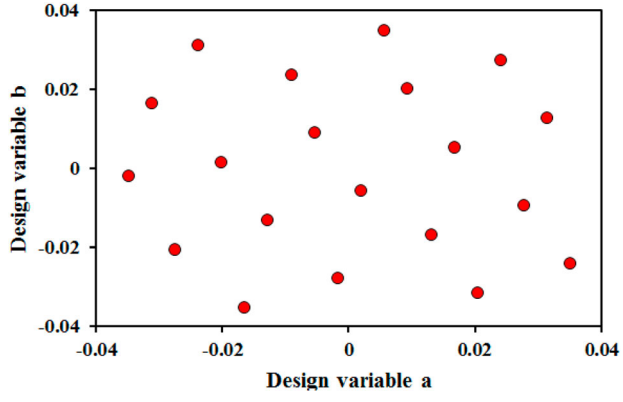

Figure 17. Sample ships distribution for the test data.

Table 5. Test samples obtained using Opt LHD method, including the corresponding draft and C_W.

No.	*a*	*b*	Draft	C_W calculated by potential theory
1	−0.0203	0.0018	0.12352	0.0014767
2	−0.0129	−0.0129	0.12307	0.0015451
3	−0.0055	0.0092	0.1253	0.001307
4	−0.0239	0.0313	0.12552	0.0012526
5	0.0055	0.035	0.1283	0.0012138
…	…	…	…	…
16	0.0018	−0.0055	0.12472	0.0013231
17	0.0166	0.0055	0.12679	0.00125
18	−0.0018	−0.0276	0.12288	0.0016162
19	−0.035	−0.0018	0.12218	0.0015985
20	−0.0166	−0.035	0.12126	0.0017784

neural networks present in Section 5.3 are used in this section to estimate the prediction results.

Figure 18 shows the prediction results by using the BP, Elman, RBF and DBN methods, respectively. As shown in Figure 18, the C_W obtained by the DBN method is much closer to the potential theory results comparing to the other three neural network algorithms.

For further illustrating the prediction performance for different methods, the RMSE, MAE and R^2 values are calculated and summarized in Table 6. As can be seen from the table, BP method has the largest RMSE, MAE and the smallest R^2, while DBN method has the smallest RMSE, MAE and largest R^2 in the prediction of C_W. As the advantage of the context layer added in the Elman method, the prediction accuracy of the Elman surrogate model is better than the BP surrogate model. In the RBF algorithm, the Gauss function is used to calculate the weight, achieving better prediction performance comparing to the BP and Elman neural networks. The RBF and DBN neural networks are two effective methods for predicting the C_W. However, the DBN method is more accurate than the RBF method in the wave-making resistance prediction. It concludes that the DBN surrogate model is a promising new surrogate model to predict the wave-making resistance for Wigley ship.

5.5. Accuracy verification for training set size

As the training set size of the surrogate model is one of the most important part in the neural network prediction. In this section, the DBN method is employed to verify the prediction results for the different training set sizes. Another three-set sizes are selected as the training samples using the Opt LHD method, the sample ships distribution for the different training sizes are shown in Figure 19. Following this, the MAD method is used to smooth the sample data. Figures 20–22 show the results for different samples.

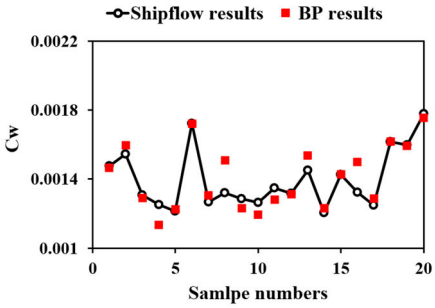

(a) A comparison of the C_W for potential theory and BP method

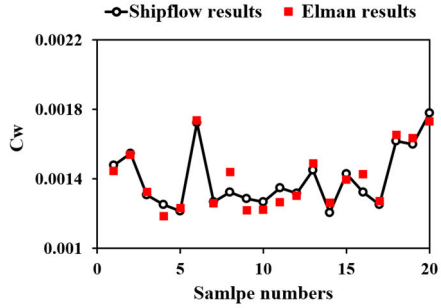

(b) A comparison of the C_W for potential theory and Elman method

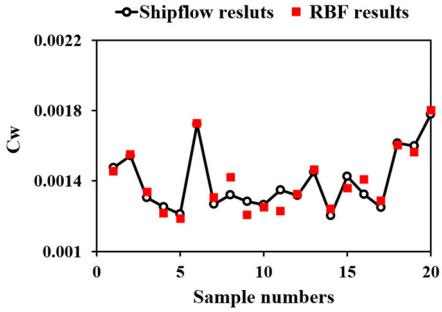

(c) A comparison of the C_W for potential theory and RBF method

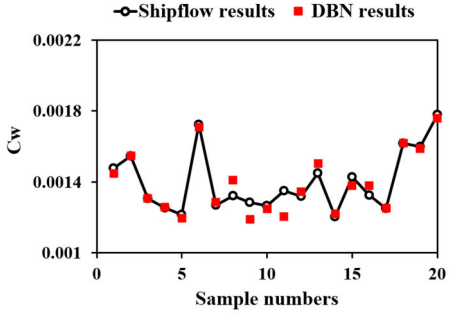

(d) A comparison of the C_W for potential theory and DBN method

Figure 18. A comparison of C_W among the different methods. (a) A comparison of the C_W for potential theory and BP method, (b) a comparison of the C_W for potential theory and Elman method, (c) a comparison of the C_W for potential theory and RBF method and (d) a comparison of the C_W for potential theory and DBN method.

Table 7 shows the prediction results for the different training sizes. As can be seen from the table, the average error calculated for 50 samples is the highest when compared to those calculated for the other three training sizes, and the error calculated for 100 samples is the lowest. The average error calculated by the 150 samples is approximately the same as the results calculated for 200 samples. The prediction results indicate that as the

Table 6. A comparison of RMSE, MAE and R^2 for the wave-making prediction.

Surrogate model	BP method	Elman method	RBF method	DBN method
RMSE	6.01 e^{-05}	4.3 e^{-05}	4.19 e^{-05}	4.05 e^{-05}
MAE	3.3 e^{-05}	2.87 e^{-05}	2.67 e^{-05}	2.21 e^{-05}
R^2	0.839	0.908	0.912	0.918

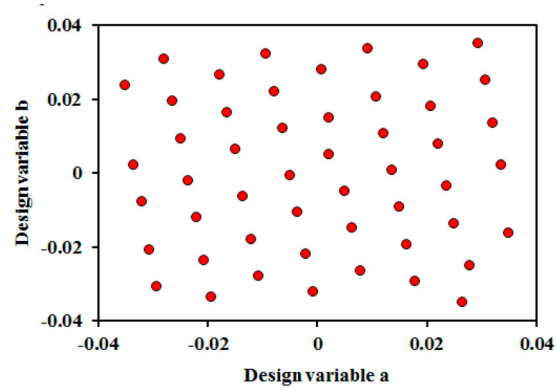

(a) 50 sample ships distribution

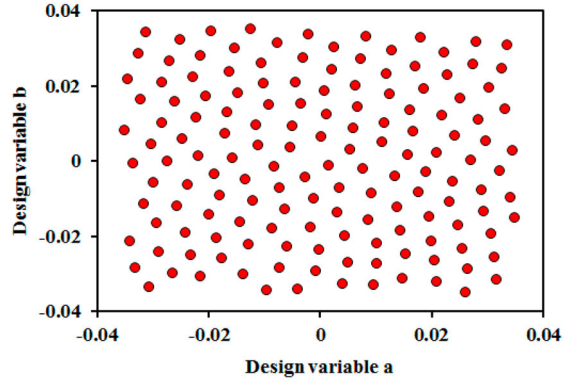

(b) 150 sample ships distribution

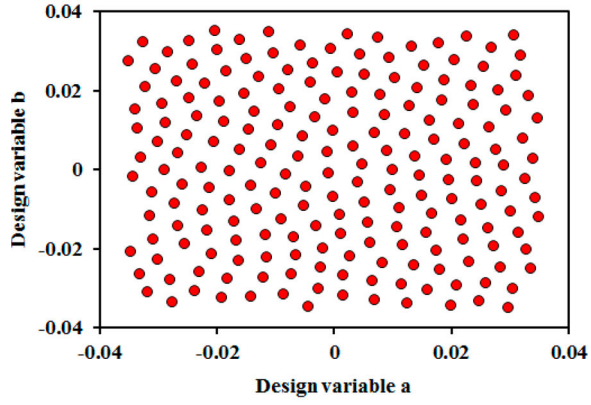

(c) 200 sample ships distribution

Figure 19. The sample ships distribution for the different training sizes. (a) 50 sample ships distribution, (b) 150 sample ships distribution and (c) 200 sample ships distribution.

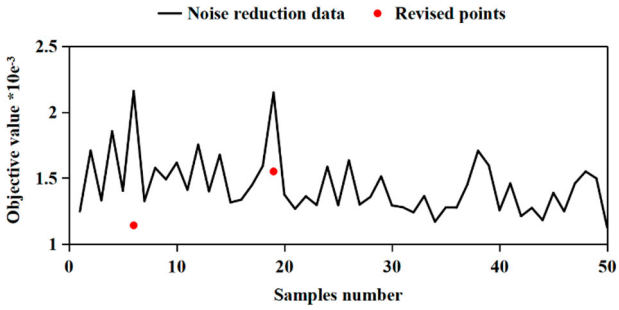

Figure 20. The filter noise for the 50 sample ships

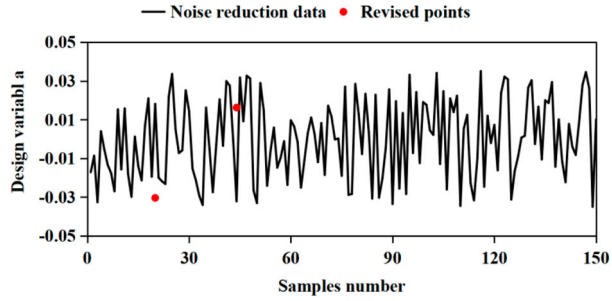

(a) The filter noise for the design variable a

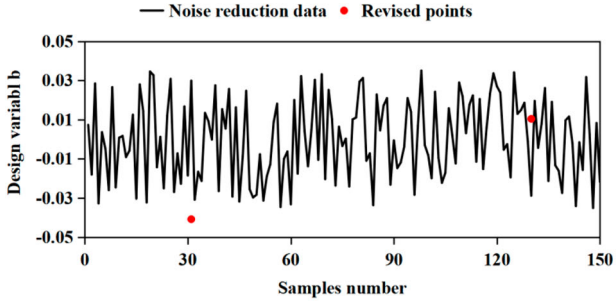

(b) The filter noise for the design variable b

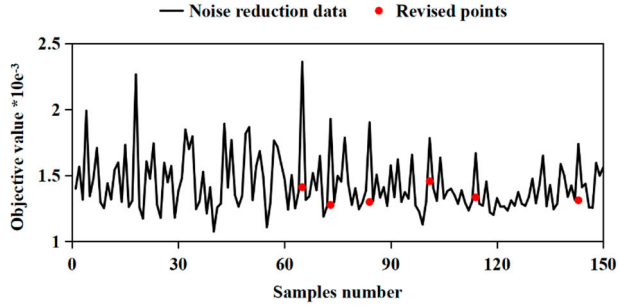

(c) The filter noise for the objective function

Figure 21. The filter noise for the 150 sample ships. (a) The filter noise for the design variable *a*, (b) the filter noise for the design variable *b* and (c) the filter noise for the objective function.

number of samples increases, the improvement in the prediction accuracy is not obvious. Furthermore, only the value of R^2 calculated for 50 samples is less than 0.9, and the prediction results calculated for the other three

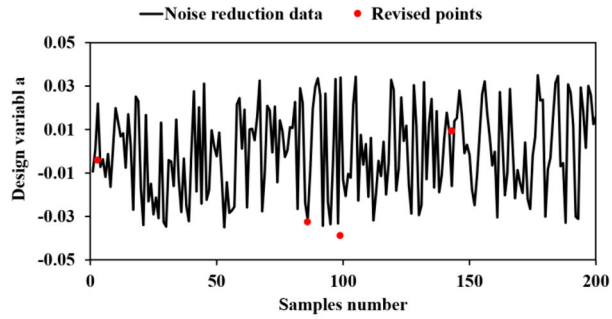

(a) The filter noise for the design variable a

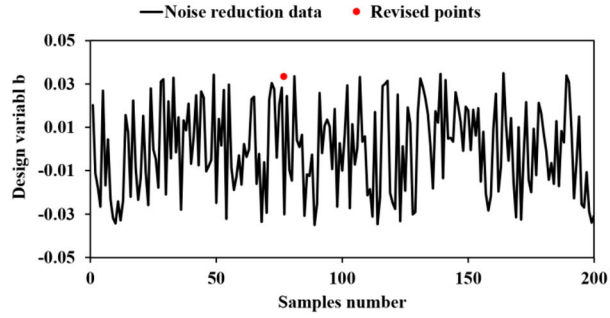

(b) The filter noise for the design variable b

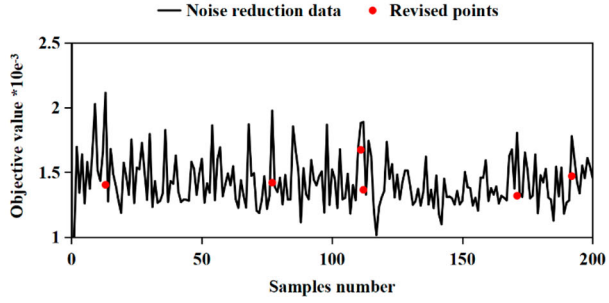

(c) The filter noise for the objective function

Figure 22. The filter noise for the 200 sample ships. (a) The filter noise for the design variable *a*, (b) the filter noise for the design variable *b* and (c) the filter noise for the objective function.

samples are greater than 0.9. The results show that after three training sizes satisfy the accuracy requirement for wave-resistance prediction, while the 100 samples show the best prediction effectiveness.

6. Optimization example

As can be seen from above, the DBN method shows good resistance prediction performance for a Wigley ship. Therefore, in this section, the ship design optimization method is established using DBN surrogate model and FFD and NLPQL methods. The optimization work is set up on the Core-i5 CPU computer. All the CFD simulations are performed using the XPAN model on the SHIPFLOW software. The NLPQL is utilized to find the optimal solution in a fix ship hull

Table 7. Prediction results for the different training sizes.

Training sizes	RMSE	MAE	R^2	Average error %
50 samples	5.52 e^{-05}	3.64 e^{-05}	0.839	3.95
100 samples	4.05 e^{-05}	2.21 e^{-05}	0.918	2.24
150 samples	4.57 e^{-05}	2.69 e^{-05}	0.901	2.963
200 samples	4.21 e^{-05}	2.64 e^{-05}	0.91	2.958

form optimization space, the initial design variables for the NLPQL algorithm are set as $a = -0.02326$, $b = -0.02513$, the wave-making resistance coefficient for the initial ship is 0.0017431.

The iterative calculations and coupling with other parameters in the ship hull form optimization can lead to significant errors for the optimization results due to the influence of the ship speeds (Hou et al., 2016). Therefore, the uncertainty optimization was also conducted in this study using the interval number method. The uncertainty level was set as 4% and 5% for the design speed. The lower bound was 1.487 m/s and the upper bound was 1.611 m/s at 4% numerical uncertainty, while the lower bound was 1.472 m/s and the upper bound was 1.627 m/s at 5% numerical uncertainty, as shown in Table 8. The objective function was set as the mean C_W of the lower and upper bounds. Table 8 also shows the optimization results using the different optimization methods. To obtain the wave-making resistance of one deformed ship, 30 s and 4 s were required using the CFD method and DBN-based method, respectively. Compared with the CFD method, the DBN-based method can effectively minimize the wave-making resistance computation time for about 10 times. The percentage of resistance reduction in Table 8 is the error between the optimal and the original ships.

According to Table 8, the certainty and uncertainty optimization methods can both obtain the optimal ship. The C_W of the optimal ship hull decreased 12.73% and 12.55% at the uncertainty level of 4% and 5%, respectively. The optimal ship hull form has the best resistance reduction at certainty optimization than the other two uncertainty levels. As the speed perturbation is added in the ship hull form optimization, the higher parameter uncertainty level leads lower optimal solution. It can be deduced that with the increase of the uncertainty level, the change of the ship speed has a certain impact on the optimal solution for the Wigley ship. However, the influence is very small. For the certainty optimization, the C_W of the optimal ship hull form decreased by 12.90% and 12.60% using the CFD and DBN methods. It can be found that the optimal solution obtained using the DBN-based optimization method is almost the same as its obtained using the CFD-based optimization method. The optimization results indicate that DBN-based ship hull form optimization can be applied to optimize the Wigley ship for reducing wave-making resistance.

Figure 23 shows the ship hull transverse lines for the original hull and optimal hull obtained by using the DBN-based optimization method. According to Figure 23, the optimal hull lines show good smoothness. The optimal hull form is inward shrinkage to achieve the reduction of the C_W. The draft for the optimal hull increases about 4.65%. The C_W of the optimal ship optimized using the DBN network is 0.00117823, and it optimized using the CFD method is 0.00117075. The deviation between the CFD method and the DBN method is only 0.638%, which further indicates that the DBN method is suitable for the wave-making resistance evaluation.

Figure 24 summaries the wave contours for original and optimal hulls. According to Figure 24, for optimal ship hull, the forward shoulder and stern waves have been sharply reduced compared to the original ship, indicating the reduction of the ship's wave-making resistance.

Figure 25 summaries C_W changes with different Froude numbers. The C_W of the optimal ship hull form has been reduced from $Fr = 0.28$ to $Fr = 0.36$ comparing to the original ship, and it achieves large reduction at $Fr = 0.28$. It can be deduced that the current optimization method can obtain the suitable ship hull form, which

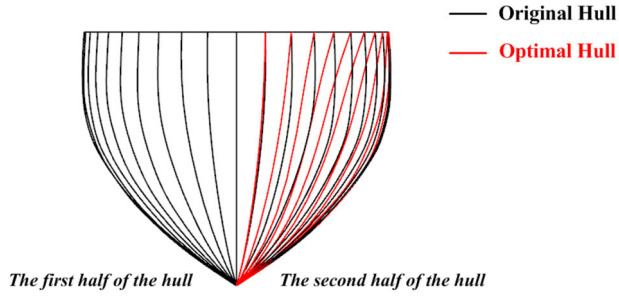

Figure 23. The transverse lines for different ship hull lines.

Table 8. Optimization results using the different methods.

No.	Optimization methods	Uncertainty level	Ship speed		Resistance reduction %
			Lower bound	Upper bound	
1	CFD certainty optimization	0	–	–	12.90
2	CFD uncertainty optimization	4%	1.487	1.611	12.73
3	CFD uncertainty optimization	5%	1.472	1.627	12.55
4	DBN surrogate model	0	–	–	12.60

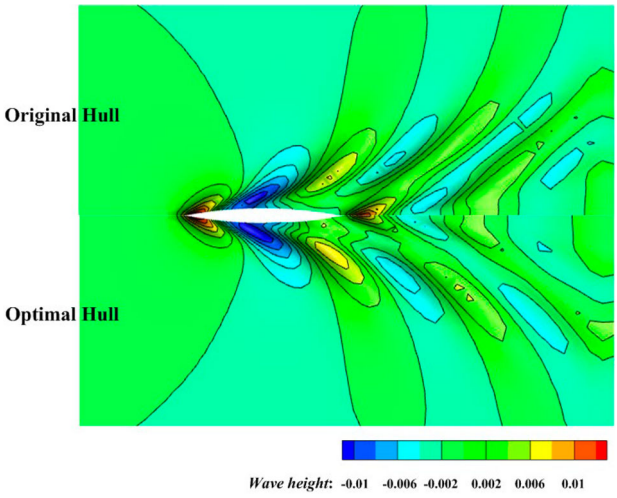

Figure 24. Details of the free surface wave contours for different ship hull form.

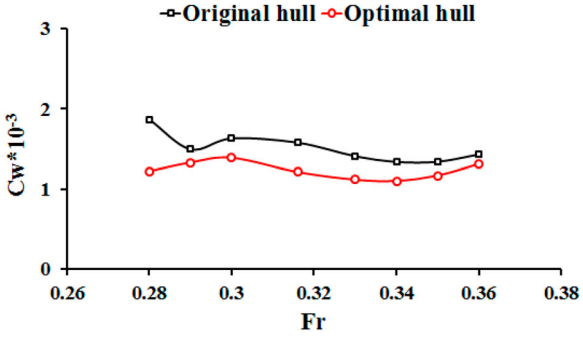

Figure 25. C_W changes with different *Fr*.

achieving the reduction in the C_W not only at design speed but also near the design speed.

7. Conclusion

A comparative analysis of BP, Elman, RBF and DBN neural networks was carried out in this study to discuss the prediction performance of the C_W firstly. The prediction results show the DBN method is better than the other three surrogate models shown in this paper in the prediction of C_W. Following this, the DBN-based ship hull form optimization platform was built for reducing the C_W of the Wigley ship, integrating the FFD and NLPQL and DBN algorithms. At the same time, the certainty and uncertainty optimization problems were also carried out and discussed. The optimization results show that with the increase of the uncertainty level, the optimization results are poor. It can be found that the ship speeds will influence the results for the CFD uncertainty optimization, while the influence is not very large. Compared with the traditional CFD optimization method, the DBN-based optimization method can also be used to optimize the Wigley ship for reducing the C_W.

The optimization platform presented is the single objective optimization problem at design speed $Fr = 0.35$ using a local optimal algorithm. Further studies will carry out the multi-speed optimization to improve the ship hydrodynamic performance at different speeds using a global optimization algorithm.

Disclosure statement

No potential conflict of interest was reported by the author(s).

Funding

This work was supported by Natural Science Foundation of Jiangsu Province [Grant Number BK20201052]; Natural Science Foundation of the Jiangsu Higher Education Institutions of China [Grant Number 19KJB580006]; National Science Foundation of China [Grant Numbers 11802039, 51009087].

ORCID

Shenglong Zhang http://orcid.org/0000-0002-9348-4395
Tahsin Tezdogan http://orcid.org/0000-0002-7032-3038

References

Baar, J. D., Roberts, S., Dwight, R., & Mallol, B. (2015). Uncertainty quantification for a sailing yacht hull, using multi-fidelity kriging. *Computers & Fluids*, *123*, 185–201. https://doi.org/10.1016/j.compfluid.2015.10.004

Bakhtiari, M., & Ghassemi, H. (2020). CFD data based neural network functions for predicting hydrodynamic performance of a low-pitch marine cycloidal propeller. *Applied Ocean Research*, *94*, 1–16. https://doi.org/10.1016/j.apor.2019.101981

Bengio, Y. (2009). Learning deep architectures for AI. *Foundations and Trends R in Machine Learning*, *2*(1), 1–127. https://doi.org/10.1561/2200000006

Bu, H. D., Gan, Y. L., Wang, Y., Zhou, S. G., & Guan, J. H. (2017). A new method for enhancer prediction based on deep belief network. *BMC Bioinformatics*, *18*(1), 99–105. https://doi.org/10.1186/s12859-017-1515-1

Chen, L. L., Guo, Z., Hou, Z. X., Deng, X. L., & Zhu, B. J. (2019). Layout design and optimization analysis of combined hypersonic vehicle. *Physics of Gases*, *4*(6), 29–39. https://doi.org/10.19527/j.cnki.2096-1642.0777

Chen, L. M. (2016). *Numerical analysis on hydrodynamic performance of catamaran in large waves*. Harbin Institute of Technology.

Cheng, X. D., Feng, B. W., Liu, Z. Y., & Chang, H. C. (2018). Hull surface modification for ship resistance performance optimization based on Delaunay triangulation. *Ocean Engineering*, *153*, 333–344. https://doi.org/10.1016/j.oceaneng.2018.01.109

Deng, L. (2014). *Lightweight research of ship structure based on the artificial neural network*. Jinan University Press.

Dong, Z. K., Liang, P. W., Zhou, C. Y., Sun, J. L., Zhao, J. Y., & Lu, M. L. (2020). Vibration prediction of hot-rolled high-strength steel sheet mill based on DBN algorithm. *Mining and Metallurgical Engineering*, *40*(4), 135–144.

Feng, M. F., & Lu, J. C. (2010). Study on short time traffic flow prediction based on RBF neural network optimized by PSO. *Computer Simulation*, *27*(12), 323–326.

Feng, X. X. (2015). *Research on image recognition based on deep learning algorithm*. Taiyuan University of Technology Press.

Garg, N., Kenway, G. K. W., Martins, J. R. R. A., & Young, Y. L. (2017). High-fidelity multipoint hydrostructural optimization of a 3-D hydrofoil. *Journal of Fluids and Structures*, *71*, 15–39. https://doi.org/10.1016/j.jfluidstructs.2017.02.001

Guo, J., Zhang, Y., Chen, Z. G., & Feng, Y. K. (2020). CFD-based multi-objective optimization of a waterjet-propelled trimaran. *Ocean Engineering*, *209*. https://doi.org/10.1016/j.oceaneng.2019.106755

Han, L. Q. (2007). *Theory, design and application of the artificial neural network*. Chemical Industry Press.

He, Z. F. (2016). *Matlab R2015b nerual network technology*. Tsinghua University Press.

Hinton, G. E., Osindero, S., & The, Y. W. (2006). A fast learning algorithm for deep belief nets. *Neural Computation*, *18*(7), 1527–1554. https://doi.org/10.1162/neco.2006.18.7.1527

Hou, Y. H., Liang, X., & Zheng, G. C. (2016). High speed vessel hull uncertainty optimization design considering the influence of speed perturbation. *Journal of Dalian Maritime University*, *42*(3), 9–14. https://doi.org/10.16411/j.cnki.issn1006-7736.2016.03.002

Huang, J. B. (2018). *Research on aero-engine exhaust gas temperature prediction*. Civil Aviation University of China Press.

Jia, B., Sun, Y. J., & Zhang, G. M. (2020). A prediction method for bounced landing of aircraft based on DBN. *China Safety Science Journal*, *30*(6), 84–91. https://doi.org/10.16265/j.cnki.issn1003-3033.2020.06.013

Kim, J. H., Kim, Y., & Lu, W. J. (2020). Prediction of ice resistance for ice-going ships in level ice using artificial neural network technique. *Ocean Engineering*, *2017*, 1–12. https://doi.org/10.1016/j.oceaneng.2020.108031

Lan, L. (2012). *Numerical calculation of wave resistance and hull lines optimization*. Harbin Engineering University Press.

Li, A. L., Zhao, D. Z., Guo, Z. B., Zhang, S., & Xie, S. F. (2020). Prediction of converter oxygen consumption in improved deep belief network. *China Measurement & Test*, *46*(6), 1–6.

Li, D., Zhou, K. F., Sun, W. D., Wang, J. L., Yu, H., & Li, H. (2015). Application of BP neural network and SVM in mine environmental assessment. *Arid Land Geography*, *38*(1), 128–134. https://doi.org/10.13826/j.cnki.cn65-1103/x.2015.01.017

Li, J. L., Wang, P., Chen, X., & Dong, H. C. (2020). Shape optimization of blended-wing-body underwater gliders based on free-form deformation. *Journal of Northwestern Polytechnical University*, *38*(3), 459–464. https://doi.org/10.1051/jnwpu/20203830459

Li, L. C., Qin, L. Q., Qu, X., Zhang, J., Wang, Y. G., & Ran, B. (2019). Day-ahead traffic flow forecasting based on a deep belief network optimized by the multi-objective particle swarm algorithm. *Knowledge-Based Systems*, *172*, 1–14. https://doi.org/10.1016/j.knosys.2019.01.015

Li, R., Xu, P., Peng, Y., & Ji, P. (2016). Multi-objective optimization of a high-speed train head based on the FFD method. *Journal of Wind Engineering and Industrial Aerodynamics*, *152*, 41–49. https://doi.org/10.1016/j.jweia.2016.03.003

Li, W. (2014). *The research and application of deep learning in image recognition*. Wuhan University of Technology.

Li, Z. M., Liang, C. X., & Wang, M. S. (2020). Short-term power generation output prediction based on a PSO-DBN neural network. *Power System Protection and Control*, *48*(8), 149–154. https://doi.org/10.19783/j.cnki.pspc.190723

Lin, Y., He, J. Y., & Li, K. (2018). Hull form design optimization of twin-Skeg fishing vessel for minimum resistance based on surrogate model. *Advances in Engineering Software*, *123*, 38–50. https://doi.org/10.1016/j.advengsoft.2018.05.010

Liu, L. W. (2019). *Study on aerodynamic drag reduction of heavy commercial vehicle shape in the styling phase*. Jilin University.

Meng, H., Bai, J. Q., Chang, M., & Zhang, Y. (2019). Study on multi-modality in aerodynamic airfoil optimization design. *Advances in Aeronautical Science and Engineering*, *10*(5), 664–672. https://doi.org/10.16615/j.cnki.1674-8190.2019.05.012

Miao, A. Q., & Wan, D. C. (2019). Multi-objective optimization of ship wave-making resistance based on MOPSO. *Chinese Journal of Hydrodynamic*, *34*(3), 291–298. https://doi.org/10.16076/j.cnki.cjhd.2019.03.003

Miao, A. Q., Zhao, M., & Wan, D. C. (2020). CFD-based multi-objective optimisation of S60 Catamaran considering demi-hull shape and separation. *Applied Ocean Research*, *97*, 1–20. https://doi.org/10.1016/j.apor.2020.102071

Moradi, A. S., Vosoughi, A. R., & Anjabin, B. N. (2020). Maximum buckling load of stiffened laminated composite panel by an improved hybrid PSO-GA optimization technique. *Thin-Walled Structures*, *160*(6), 107382. https://doi.org/10.1016/j.tws.2020.107382

Ozcanan, S., & Atahan, A. O. (2019). RBF surrogate model and EN1317 collision safety-based optimization of two guardrails. *Structural and Multidisciplinary Optimization*, *60*(1), 343–362. https://doi.org/10.1007/s00158-019-02203-z

Shan, W. P. (2015). *Classification and recognition of transmission fault based on deep belief network*. South China University of Technology Press.

Shen, Y., Huang, W., Yan, L., & Zhang, T. T. (2020). Constraint-based parameterization using FFD and multi-objective design optimization of a hypersonic vehicle. *Aerospace Science and Technology*, *100*, 1–12. https://doi.org/10.1016/j.ast.2020.105788

Shi, X. H. (2006). *Some theoretical studies of Elman neural networks and evolutionary algorithms and their applications*. Jilin University Press.

Song, B. Y., Wang, Z. D., & Zou, L. (2021). An improved PSO algorithm for smooth path planning of mobile robots using continuous high-degree Bezier curve. *Applied Soft Computing*, *100*, 106960. https://doi.org/10.1016/j.asoc.2020.106960

Song, X., Yu, P. X., Bai, J. Q., Han, X., & Peng, J. H. (2020). Aerodynamic and aeroacoustic optimization of propeller based on Hanson noise model. *Journal of Northwestern Polytechnical University*, *38*(4), 685–694. https://doi.org/10.1051/jnwpu/20203840685

Wang, F. (2015). *Retrieval and recommendation system of resources based on deep belief networks*. Beijing University of Posts and Telecommunications Press.

Wang, X. J., Song, B. W., Wang, P., & Sun, C. (2018). Hydrofoil optimization of underwater glider using free-form deformation and surrogate-based optimization. *International Journal of Naval Architecture and Ocean Engineering*, *10*(6), 730–740. https://doi.org/10.1016/j.ijnaoe.2017.12.005

Wei, X., Chang, H. C., Feng, B. W., Liu, Z. Y., & Huang, C. R. (2019). Hull form reliability-based robust design optimization combining polynomial chaos expansion and maximum entropy method. *Applied Ocean Research*, https://doi.org/10.1016/j.apor.2019.101860.

Xu, D. Y., Bai, J. Q., & Lei, Y. Y. (2019). An aerodynamic shape optimization on design of the full configuration considering nacelle installation parameters. *Journal of Xian Jiaotong University*, *53*(4), 150–157.

Yadav, R.K., & Anubhav, A.. (2020). PSO-GA based hybrid with Adam optimization for ANN training with application in medical diagnosis. Cognitive Systems Research, 64:191–199. https://doi.org/10.1016/j.cogsys.2020.08.011

Yang, X. (2020). *Fluid mechanics simulation and hull shape optimization of yacht based on CFD*. University of Electronic Science and Technology of China.

Yang, X. H., & Zhong, N. W. (2016). Forecasting of hospital outpatient based on deep belief network. *Computer Science*, *43*(11A), 26–30.

Ye, M., Feng, B. W., & Chang, H. C. (2020). Optimization of resistance performance of deadweight tonnage 46000t oil tanker based on approximate model. *Marine Technology*, *3*(1), 6–12. https://doi.org/10.24843/JMRT.2020.v03.i01.p02

Yu, L., Chang, X., & Hu, A. K. (2016). A hydrodynamic optimization design methodology for a ship bulbous bow under multiple operating conditions. *Engineering Applications of Computational Fluid Mechanics*, *10*(1), 331–346. https://doi.org/10.1080/19942060.2016.1159987

Zhang, B. J., & Zhang, Z. X. (2015). Research on theoretical optimization and experimental verification of minimum resistance hull form based on Rankine source method. International Journal of Naval Architecture and Ocean Engineering, *7*(5), 785–794. https://doi.org/10.1515/ijnaoe-2015-0055

Zhang, Q., Chen, G., Zhang, L. J., Cao, K., & Duan, F. (2019). Research on hull lines optimization of drilling ship and additional resistance of Moonpool. *Journal of Wuhan University of Technology*, *43*(2), 327–331.

Zhang, Q., Zhu, G. B., Hu, X., & Yang, R. (2019). Adaptive neural network auto-berthing control of marine ships. *Ocean Engineering*, *177*, 40–48. https://doi.org/10.1016/j.oceaneng.2019.05.015

Zhang, R. E., Zhang, S. W., Yang, J. H., & Lu, Y. J. (2018). Three-dimensional inverse design method of centrifugal pump Balade based on free from deformation. *Journal of Engineering Thermophysics*, *39*(1), 98–103.

Zhang, S., Chen, B., Ju, F., & Xi, W. Q. (2021). Optimization of construction robot's operation point based on GA-PSO. *Electrical Automation*, *50*(01|1), 164–167. https://doi.org/10.19344/j.cnki.issn1671-5276.2021.01.042

Zhang, S. L., Zhang, B. J., Tezdogan, T., Xu, L. P., & Lai, Y. Y. (2018). Computational fluid dynamics-based hull form optimization using approximation method. *Engineering Applications of Computational Fluid Mechanics*, *12*(1), 74–88. https://doi.org/10.1080/19942060.2017.1343751

Zhang, X. (2016). *Simulation research of deep learning in wind turbine blade structural damage identification*. Lanzhou Jiaotong University Press.

Zhou, T., Jin, J. L., Li, R. B., Ji, C. M., & Li, J. Q. (2017). Performance optimization analysis for inflow prediction using wavelet support vector machine. *Journal of Hydroelectric Engineering*, *36*(10), 45–55.